Toward the elimination of bias in satellite retrievals of sea surface temperature 1. Theory, modeling and interalgorithm comparison

JOURNAL OF GEOPHYSICAL RESEARCH, VOL. 104, NO. C10, PAGES 23,565–23,578, OCTOBER 15, 1999

Toward the elimination of bias in satellite retrievals of sea surface temperature 1. Theory, modeling and interalgorithm comparison

C. J. Merchant[1]

Department of Space and Climate Physics, University College London, Mullard Space Science Laboratory, Holmbury St. Mary, Dorking, Surrey, England

A. R. Harris

U.K. Meteorological Office, Bracknell, Berks, England

M. J. Murray and A. M. Závody[2]

Space Science Department, Rutherford Appleton Laboratory, Chilton, Didcot, Oxon, England

Abstract. The along-track scanning radiometer (ATSR), launched in July 1991 on ERS-1, is an infrared radiometer designed to permit retrieval of skin sea surface temperature (SST) to the accuracy required for many climate research purposes. Using the prelaunch retrieval scheme, this accuracy (0.3 K) was achieved only when observations at 3.7 μm were available, i.e., SSTs derived from nighttime scenes before the failure of this channel in May 1992. Retrievals using only channels at 11 and 12 μm suffered significant biases. First, cold biases of up to 1.5 K arose from the radiative effects of the unanticipated presence of a significant loading of stratospheric aerosol following the eruption of Mount Pinatubo in June 1991. Second, cold biases of up to 0.4 K were associated with regions of high water vapor loading. We solve the first problem by choosing retrieval coefficients to be orthogonal to the modeled changes in brightness temperatures caused by variations in stratospheric aerosol optical depth. We attribute the second problem to deficiencies in radiative transfer modeling of water vapor continuum absorption and show that use of an updated parameterization reduces bias from wet atmospheres. Applying the new retrieval coefficients to ATSR data, we find good consistency between SSTs retrieved with and without the 3.7 μm channels, the global mean and standard deviation of differences between retrievals being of the order of 0.05 K and 0.25 K, respectively. We therefore anticipate that reprocessing ATSR data using our new retrieval scheme will result in a substantially improved record of ATSR SST, in that the following should be reduced to insignificant levels: (1) the artefactual trend (previously ~0.25 K yr^{-1} in tropical regions) corresponding to the decaying load of post-Pinatubo aerosol, (2) the discontinuity in SST retrievals (previously up to 0.7 K) associated with the failure of the 3.7 μm channel, and (3) cold biases (previously ~0.4 K) in wet tropical regions. Thus this work represents a significant advance in terms of the quality of ATSR SSTs for climate research. The techniques are also applicable to both the ATSR-2, flying on ERS-2, and the advanced ATSR (planned for launch on the Envisat platform in 2000). However, we note that even with the improved physical modeling on which the new retrieval coefficients are based, we do not yet meet the stringent requirement of 0.1 K $decade^{-1}$ stability in retrievals for climate change detection purposes.

1. Introduction

The measurement of sea surface temperature (SST) is essential to understand and monitor global climate. Radiative, sensible, and latent heat fluxes are largely governed by SST, and these fluxes, in turn, drive the general atmospheric circulation and determine important climatic features such as large-scale convection in tropical regions [e.g., *Webster*, 1994]. SST measurements need to be accurate to a few tenths of kelvin to monitor El-Nino-Southern-Oscillation events, in which regional SST anomalies of a few kelvin are associated with global effects on climate (see *Allan et al.* [1996] for a recent review). Monitoring SST for climate change purposes requires stability in the observing system of 0.1 K $decade^{-1}$ [*Allen et al.*, 1994].

The retrieval of SST from satellite measurements offers the advantage of global coverage and has been performed routinely since 1981 by the advanced very high resolution radiometer (AVHRR) to a point accuracy of ~0.5 K [e.g., *McClain et al.*, 1985; *McClain*, 1989]. In July 1991, the first along-track scanning radiometer (ATSR) was launched on the European Space

[1]Now at Department of Meteorology, University of Edinburgh, Edinburgh, Scotland.

[2]Now at Albinus Ltd, Slough.

Paper number 1999JC900105.
0148-0227/99/1999JC900105$09.00.

Agency's ERS-1 satellite. The principal purpose of the ATSR was to permit retrieval of SST to an accuracy of 0.25 K (1 standard deviation of the average over an area ~50 km^2 under conditions of up to 80% cloud cover [*Delderfield et al.*, 1986]). Like AVHRR, ATSR has thermal channels at 3.7, 11, and 12 μm and a ground resolution of ~1 km. The unprecedented design accuracy of ATSR was achieved by three technical advances. (1) Each location in the ATSR swath was viewed twice: first at ~55° zenith angle (referred to as the forward view), and then about 2 min later at ~0° (the nadir view). This dual-view capability allows better account to be taken of atmospheric absorption and emission of thermal radiation. (2) Onboard blackbody sources provided calibration of the radiometer to a 3σ accuracy of <0.1 K throughout the mission lifetime, an exceptional radiometric accuracy [*Mason et al.*, 1996]. (3) Thermal infrared detectors were cooled by an active Stirling cycle cooler to between 90 and 95 K during the early part of the mission. Consequently, the noise equivalent differential temperatures for the 3.7, 11, and 12 μm channels were approximately 0.04, 0.05, and 0.07 K respectively [*Harris and Saunders*, 1996].

Coefficients for linear retrieval of SST are derived either by direct regression of observed brightness temperatures against buoy measurements (e.g., *McClain et al.* [1985] for AVHRR), or by regression of brightness temperatures calculated for a variety of SSTs and atmospheric states using a forward model (e.g., *Závody et al.* [1995] for ATSR). The relative merits of these approaches are discussed by *Minnett* [1990]. The attraction of the empirical approach is its use of real data, eliminating possible errors from deficiencies in forward modeling. However, the empirical data consist of area-average satellite observations matched, often loosely, in time and space to point in situ measurements. Moreover, the in situ measurements are of bulk SST, whereas the radiometer is sensitive to the radiation emitted from the uppermost ~50 μm, well within the thermal skin layer. Thus, AVHRR bulk SST estimates include some random error from variability in the skin-bulk difference. The ATSR retrievals are of skin SST, since the radiometric temperature of the surface is specified in the forward model. An approach based on physical modeling allows the specification of representative conditions, avoiding the problems of obtaining sufficiently numerous and representative matchups. On the other hand, it relies on having an accurate forward model.

Validation of skin SST retrievals is difficult and costly. *Barton et al.* [1995] and *Thomas and Turner* [1995] measured SST radiometrically from ships coincident with ATSR overpasses. Despite the significant effort involved, the combined number of coincidences obtained under clear skies was only 30. Moreover, the accuracy of the radiometric measurements (~0.2 K) was comparable with the target accuracy of ATSR SSTs and therefore does not allow a stringent test. Nonetheless, Barton et al. were able to detect a relative bias of ~0.4 K between SST retrievals made with and without the 3.7 μm channel, those derived without being cooler. A similar result was found by *Mutlow et al.* [1994] using 220 globally distributed quality-controlled buoy matchups. These interalgorithm biases imply the existence of absolute biases in at least some ATSR SST retrievals. *Murray et al.* [1998b] discuss more fully the spatial and temporal nature of biases in ATSR SST retrievals using different channels.

In the ATSR scheme, bias in the SST retrieved from clear-sky brightness temperatures can arise from use of an unrepresentative sample of atmospheric and surface states, or from inadequate modeling of the corresponding brightness temperatures. We find that biases in the original SST retrievals of *Závody et al.* [1995] arose by both these mechanisms. First, the eruption of Mount Pinatubo in the Philippines, shortly before the launch of ERS-1, rendered invalid the assumption of Závody et al. that the stratosphere could be characterized as aerosol free. This was the most significant cause of SST bias (up to ~1.5 K) in the first year of the ERS-1 mission. Second, bias arose from inadequate parameterization of the water vapor continuum absorption in the 10-13 μm window region. This bias was smaller than that from stratospheric aerosol (up to ~0.4 K) but would be present throughout the mission lifetime. Other factors (the modeled effect of wind speed on surface emissivity, the concentrations previously assumed for radiatively active gases, and the distribution of atmospheric states used) may have caused biases of less than 0.1 K. Note that ineffective cloud screening is a potential source of biased retrievals [e.g., *Jones et al.*, 1996] which is not addressed in this paper.

In this paper, we establish that these interalgorithm biases present in early ATSR SSTs can be nearly eliminated. We present a straightforward, rigorous, and general method for designing SST retrievals which are negligibly biased by stratospheric aerosols; we use an updated parameterization of the water vapor continuum absorption, thereby reducing residual biases further; and we address the other minor factors listed above. As a result, biases between SSTs derived from real data with and without the 3.7 μm channel are reduced to ~0.05 K, a remarkable degree of consistency. While this consistency is a strong indication that the retrievals are of high quality, it does not establish their absolute accuracy. A companion paper [*Merchant and Harris*, this issue] describes a validation exercise in which retrieved SSTs are compared with in situ measurements. This exercise confirms the ability of the new retrieval scheme to deal with stratospheric aerosol and high water vapor loading, and demonstrates that the retrievals are unbiased to ~0.2 K.

We proceed as follows. In section 2 we first describe the radiative transfer model (RTM) and the set of atmospheric and surface states we use to develop the SST retrieval scheme. Factors which may otherwise have lead to minor biases (≤0.1 K) are dealt with here. Sections 3 and 4 describe our work on the more significant sources of SST bias. In section 3 we investigate the bias caused by stratospheric aerosols. The nature of such aerosols is described, and their effects on brightness temperatures succinctly characterized. This leads to a clear formulation of what is required for an SST retrieval scheme to be aerosol robust (i.e., to give retrievals unaffected by the aerosol) and the mathematical development of how this can be achieved. In section 4 we show that the water vapor continuum absorption in the 11 and 12 μm channels is better described by the updated parameterization. In section 6 we show that the retrieval coefficients we derive (presented in section 5) give highly consistent results when applied to measured brightness temperatures. We conclude in section 7 with a discussion of the results and future directions of research.

2. Radiative Transfer Modeling

Infrared retrievals of SST from satellite data are made using regions of the electromagnetic spectrum where the atmosphere is relatively transparent: around 3.7 μm and 10 to 13 μm. Even in these "window" regions, the brightness temperature of the radiation reaching the satellite sensor is typically lower by 1 to 10 K than would be the case were the atmosphere completely transparent. The temperature deficit is wavelength dependent. For a particular wavelength the deficit is dependent on the vertical distribution of water vapor (the main absorbing species in the window region) and the profiles of pressure and temperature in the atmosphere, that is, on the atmospheric state. The emissivity, and hence the relationship between SST and thermal emission, depends indi-

rectly on the surface wind speed. The development of a retrieval scheme based on physical modeling therefore requires the ability to calculate ATSR brightness temperatures given a description of the state of the sea surface (skin temperature and wind speed) and the profile of temperature, humidity and pressure in the atmosphere. We use the line-by-line RTM previously employed by *Závody et al.* [1995], with the following minor modifications.

1. The parameterization of sea surface emissivity against wind speed, formerly that of *Masuda et al.* [1988], is now that of *Watts et al.* [1996]. The new emissivities are channel-integrated rather than midchannel values. More important, the emissivity is enhanced in the forward look direction at high wind speeds because the parameterization accounts for radiance emitted and then reflected by another facet of the rough sea surface into the look direction.

2. Instead of the previous assumption of specular reflection at the sea surface, downwelling radiance at the specular angle is multiplied by an "enhancement factor" (≥1.0) to find the corresponding upwelling reflected radiance. This accounts for the effects of double reflections and the anisotropy of downwelling radiance. The factor is essentially 1.0 for near-nadir and low wind speed cases. We modify the original parameterization of *Watts et al.* [1996], which was in terms of surface-to-top-of-atmosphere transmission, and use instead the total column water vapor, as in fact, suggested by *Watts et al.* [1996].

3. The concentration of carbon dioxide is set at 355 ppmv, as is more appropriate to 1991 [*Watson et al.*, 1992].

4. The extinction and absorption coefficients (σ_e and σ_a, respectively) and asymmetry parameter g used for modeling the radiative effects of tropospheric and stratospheric aerosols are updated to correspond to the tabulated values in the radiative transfer code, MODTRAN3. A first-order approximation is adopted to account for aerosol scattering into the view direction, an effect previously neglected. In this approximation, an net extinction coefficient, σ_{net}, is found by interpolating σ_e and σ_a with respect to g: $\sigma_{net} = \sigma_e - ((g+1)/2)(\sigma_e - \sigma_a)$. Physically, this represents the fact that scattering by the aerosol out of the view direction is compensated by scattering into the view direction to a degree dependent on the asymmetry between forward and backward scattering. This approximation is very good for stratospheric aerosol, since the optical depths involved are small (<<0.1), and downwelling radiance is negligible.

We also seek to improve on *Závody et al.* [1995] in terms of the range and representativeness of atmospheric profiles and surface states used. We select gridded initialized data from the European Centre for Medium-range Weather Forecasts (ECMWF) Re-Analysis (ERA) project for 4 months (October 1991, January 1992, April 1992, and August 1992) for each of four dates and times (1st of the month at 0000 hours, 7th at 1200, 15th at 0600 and 23rd at 1800). At each oceanic point on the latitude-longitude grid we use the following data to specify the state: skin temperature, sea level pressure, 10-m wind speed, 2-m air temperature and dew-point, and profile of temperature and relative humidity at each of the 16 pressure levels between 1000 and 10 hPa. The ERA 2.5° grid is further subsampled to a basic interval of 15° but using greater intervals of longitude at high latitudes to approximate equal area weighting. Since ATSR measures SST under clear skies only, we exclude states which are nominally cloudy by requiring that the relative humidity be <95% for all levels. States are also excluded if the skin temperature is < 271.35 K, representing ice cover on the sea surface. The resulting data set consists of 1358 states. All oceanic regions, seasons, and synoptic times are represented, with the associated variations in all variables, including air-sea temperature difference and wind speed, accounted for. The distributions of SST, clear-sky total precipitable water (TPW) and air-sea temperature difference (ASTD) in the data set are shown in Figure 1. The distribution of SST is highly asymmetric, with a sharp cutoff at warm temperatures: the modal SST (~40% of states) is about 300 K, yet <4% of states have SSTs in excess of 302.5 K. The TPW distribution is much flatter, since a wide range of TPW is associated with higher SSTs, from wet profiles in the tropical warm pool region, to relatively dry profiles in regions of subsidence. Over 95% of ASTDs are in the range -4 to +2 K, which matches the range of ASTDs found in a study of 160 AVHRR-buoy matchups by *May and Hoyler* [1993]. More negative differences occur, particularly at high latitudes and coastal regions. The difference between the brightness temperature and SST for a particular channel and state varies principally with the amount of water vapor present and the difference in temperature between the sea surface and the absorbing constituents in the atmosphere. This is illustrated in Figure 1(d), where the average 11 μm nadir temperature deficits calculated for the data set are plotted as functions of ASTD and TPW. Increased water vapor in the atmosphere increases the deficit of the brightness temperature below the SST because of increased absorption. Cooler atmospheres (relative to the SST) are associated with increased temperature deficits because their atmospheric thermal emission is smaller.

By using ERA data, we depart from the previous practice of relying on radiosonde profiles. The clear advantage is that oceanic regions, which are sparsely sampled by radiosondes, are appropriately represented in the regression. However, *Soden and Bretherton* [1994] concluded that the ECMWF model is deficient in upper tropospheric humidity (UTH) in areas of strong convection and has excess UTH in regions of subsidence. UTH significantly affects the outgoing radiance in the 10-13 μm region [e.g. *Minnett*, 1986]. For the dual-view two-channel and dual-view three-channel coefficients derived in this paper, we find that changing the relative humidity between 5 and 12 km by ~15% introduces biases of only ~0.04 and ~0.01 K, respectively, into the retrieved SSTs. The range of humidity in the ERA data seems sufficiently wide to render the retrievals fairly insensitive to possible biases. In any case, given the choice between radiosondes and reanalysis data, the difficulties radiosondes have in measuring UTH should be remembered [e.g. *Soden and Lanzate*; 1996, *Balagurov et al.*, 1998; *Schmidlin*, 1998].

3. Eliminating Bias From Stratospheric Aerosol

3.1. Effect of Stratospheric Aerosols on Brightness Temperatures

Major volcanic eruptions can increase the stratospheric aerosol mass loading by 10-fold or more over background levels, the three most recent events of this magnitude being Agung in 1963, El Chichon in 1982, and Pinatubo in 1991 [*McCormick et al.*, 1993]. Lesser eruptions can increase the mass loading less dramatically but still significantly. After injection into the stratosphere, the volcanic matter chemically evolves, is dispersed zonally and meridionally, and undergoes sedimentation. After the Pinatubo eruption, *McCormick and Veiga* [1992] found that within 3 weeks the plume had encircled Earth, most of the mass being in the band between 10°S and 30°N and at heights of 20 to 25 km. At this stage the "fresh" plume consisted of sulfur dioxide gas, crustal particles, and the first droplets produced by conversion of sulfur dioxide to sulfuric acid with a characteristic timescale of ~35 days [*Bluth et al.*, 1992]. The stratospheric aerosol dispersed poleward over a

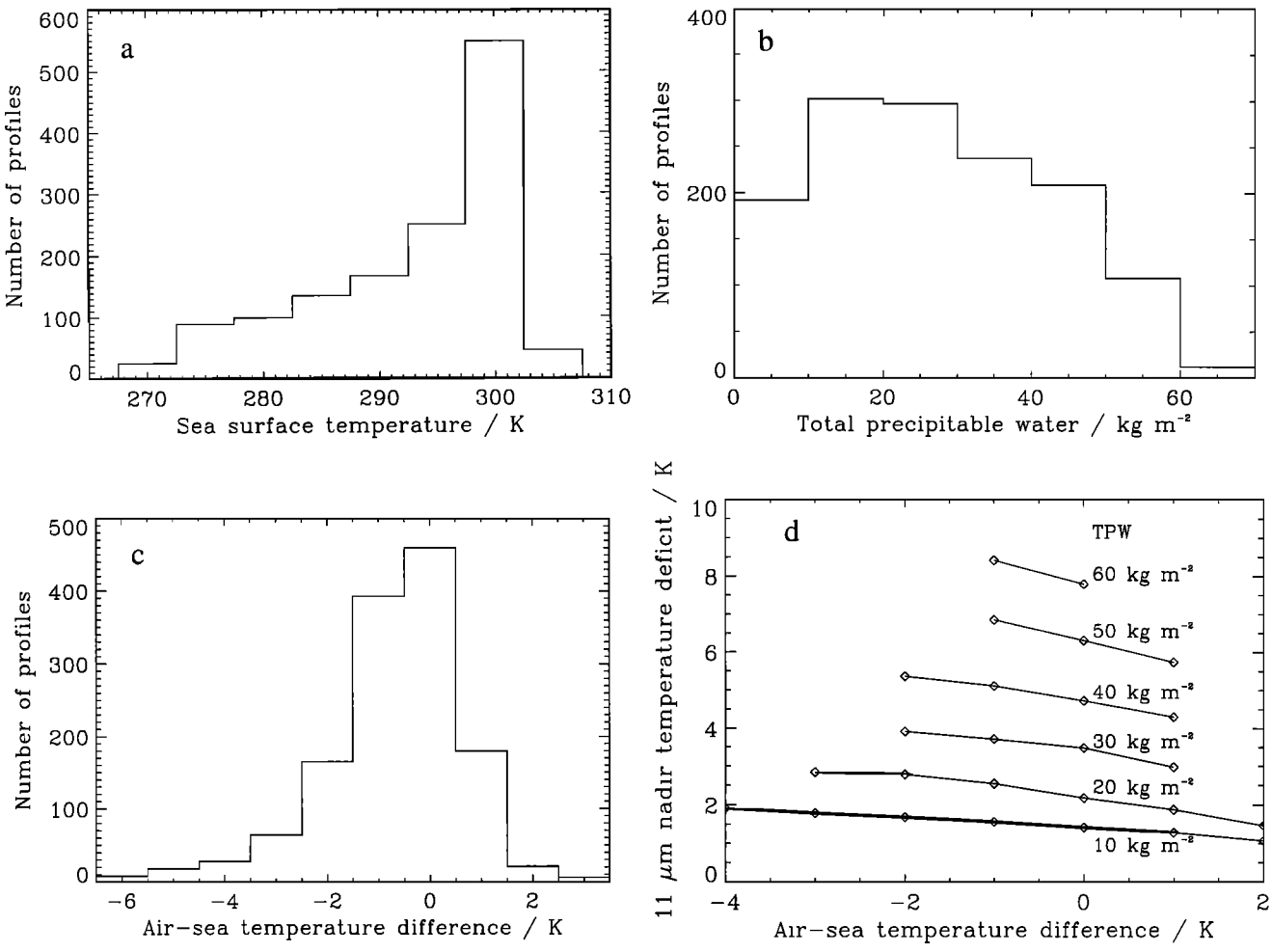

Figure 1. Characteristics of data set of surface and atmospheric states and calculated brightness temperatures. (a) Distribution of SST. (b) Distribution of TPW. (c) Distribution of ASTD. (d) Dependence of 11 μm nadir temperature deficit on TPW and ASTD.

timescale of a few months to 1 year [*Trepte et al.*, 1993], with the total stratospheric aerosol mass loading decreasing by sedimentation from a maximum in September 1991 to preeruption levels by October 1993 [*Baran and Foot*, 1994]. A "background" sulfuric acid aerosol may persist in the stratosphere without volcanic input [*Hamill et al.*, 1997].

Thus we may characterize stratospheric aerosols as broadly of three types: "fresh volcanic," typical of the plume shortly after the eruption, with a lifetime of the order of one month and whose distribution is relatively localized; "aged volcanic aerosol," which may disperse round the globe and has a lifetime of the order of 1 year; and "background aerosol," present many years after major eruptions. Differences in chemical composition and particle size distribution between these types give rise to distinct infrared radiative characteristics.

Stratospheric aerosol interacts with upwelling terrestrial infrared radiation by absorption and scattering and also emits its own thermal radiation. *Baran and Foot* [1994] calculated that the transmission through a layer of stratospheric aerosol representing the fresh Pinatubo plume to be 0.99 at 12 μm, corresponding to an optical depth of 0.01, and *Lambert et al.* [1993] estimated from infrared limb-sounding measurements that in November 1991 the global mean optical depth at 12.1 μm was 0.0055. Thus the stratospheric aerosol layer is optically thin, and consequently, there is a near-linear relationship between the optical depth of stratospheric aerosol and the depression of brightness temperature observed by ATSR. This is illustrated in Figure 2a for "aged volcanic" aerosols and calculated brightness temperature deficit in the 3.7 μm channel, nadir view. The ordinate of each point corresponds to the difference between brightness temperatures calculated with and without stratospheric aerosol present for a single atmospheric and surface state. Every fifth state of the 1358 states is used to give a representative subset of states for the simulation of aerosol effects. The amounts of stratospheric aerosol are randomly allocated to the states and give rise to the optical thickness in the 12 μm channel (nadir view) plotted on the abscissa. The radiance absorbed and scattered by the aerosol is proportional to both the amount of aerosol and the upwelling radiance. The latter is largely determined by the surface temperature and contributes to the scatter of points. Similar effects are apparent in Figures 2b and 2c, where the temperature deficit for the 11 μm channel (nadir view) and 12 μm channel (forward view), respectively, are plotted. Variations in surface temperature affect the radiance in all channels, so when the temperature deficits are plotted against the 12 μm (nadir) temperature deficit (Figures 2d to 2f), the points lie more tightly on a straight line. The residual scatter around the best fit straight line

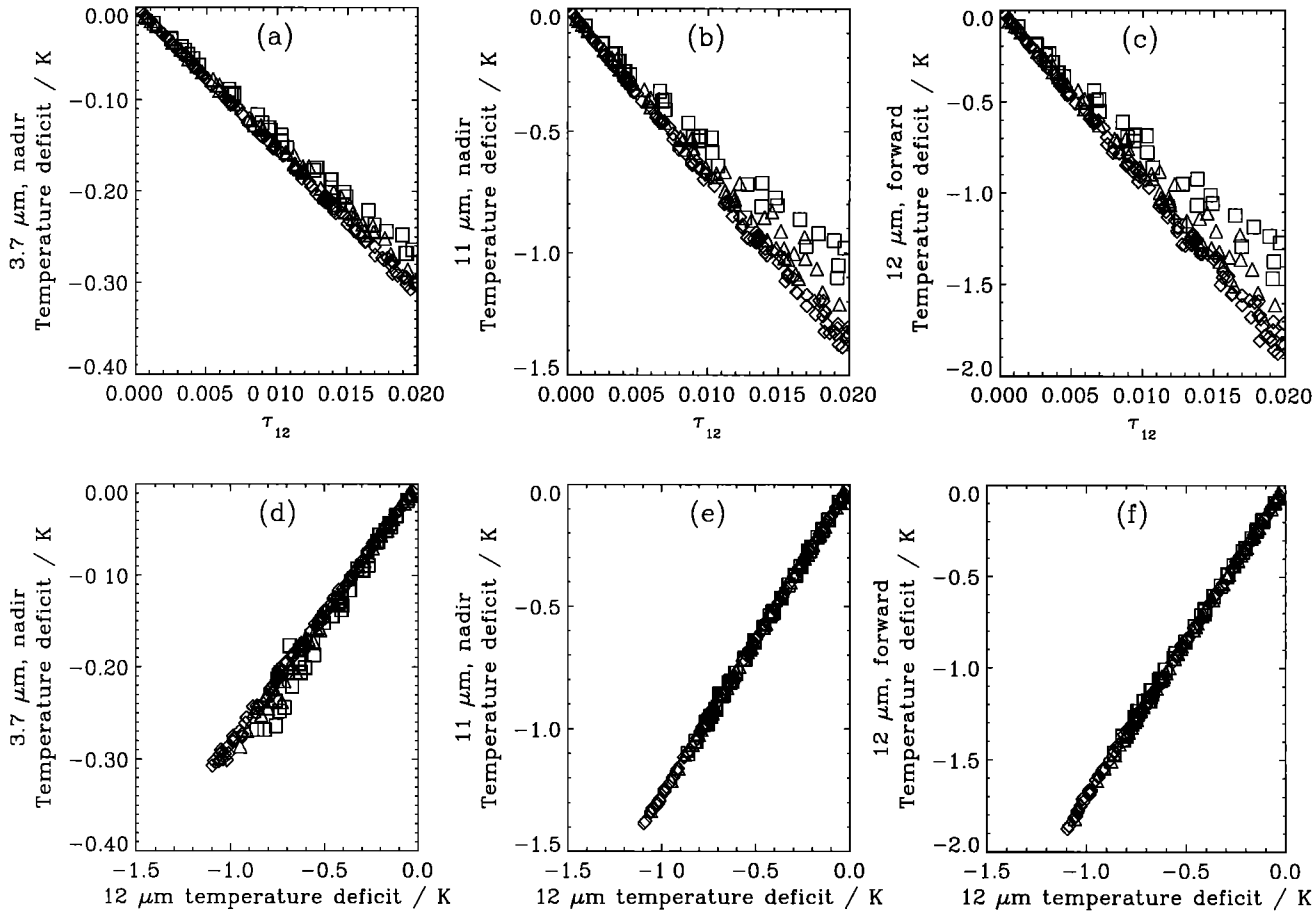

Figure 2. Calculated changes in brightness temperature from the presence of varying amounts of stratospheric aerosol. Diamonds indicate SST greater than 295 K, triangles indicate SST between 285 and 295 K, and squares indicate SST less than 285 K. (a): Temperature deficit in 3.7 μm channel, nadir view, against optical thickness of aerosol in the 12 μm channel (nadir). (b, c): Same as Figure 2a, except for temperature deficits in the 11 μm nadir and 12 μm forward channels respectively. (d to f) Same as Figures 2a to 2c, except temperature deficits are plotted against the 12 μm nadir temperature deficit. Note the changes in scale of the vertical axis.

through the points in Figure 2d is 8% and is less than 1% for Figures 2e and 2f. The residual is greatest for the 3.7 μm channel because of the considerably steeper Planck-function dependence of radiance on temperature at this wavelength. Most of the 8% scatter in Figure 2d is associated with high-latitude states with low SSTs; for states with SSTs greater than 285 K, the corresponding scatter is 3%. Similar results apply for the channels and views not shown and for fresh volcanic and background aerosols. The technique we present for finding aerosol-robust SST coefficients is based on the nearly proportional relationship between temperature deficits in different channels.

The effect of stratospheric aerosol on ATSR brightness temperatures can therefore be described by the "modes" of temperature variation shown in Figure 3. This figure shows the relative temperature deficits in the three ATSR channels for both look angles at center swath. It also shows the order of magnitude of deficits caused by indicative amounts of fresh and aged volcanic aerosol (optical depth in the 12 μm channel, τ_{12}=0.01) and background aerosol (τ_{12} = 0.001). The modes for fresh and aged aerosol are similar, with the deficit in the 11 and 12 μm channels being comparable (about 30% greater in the 11 μm channel) and that in the 3.7 μm channel being much smaller. For background aerosol the

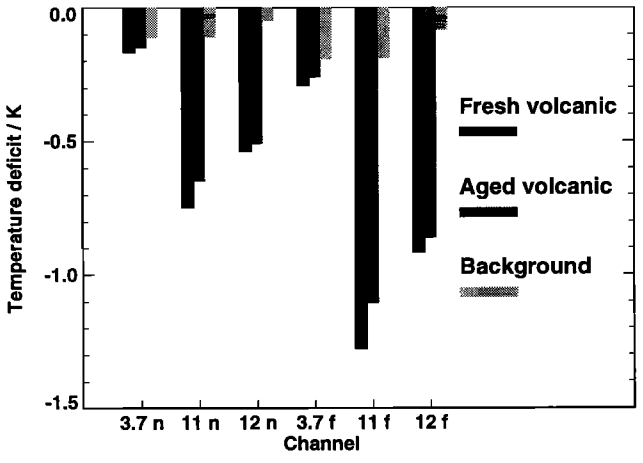

Figure 3. Modes of variation introduced by stratospheric aerosol of different types into ATSR brightness temperatures observed at center swath. The temperature deficits shown are for a 12 μm optical depth of 0.01 for fresh and aged volcanic aerosol and 0.001 for background aerosol, and are average values for a globally representative subset of atmospheric and surface states.

Table 1. Descriptors of the Effect of Stratospheric Aerosol on Brightness Temperatures

	Term	Fresh Volcanic	Aged Volcanic	Background
		Center of Swath		
c		-186	-166	-329
k	3.7 n	0.091	0.091	0.343
	3.7 f	0.158	0.158	0.592
	11 n	0.403	0.392	0 337
	11 f	0.689	0.669	0.573
	12 n	0 291	0.307	0.153
	12 f	0 495	0.521	0.259
		Edge of Swath		
c		-182	-162	-322
k	3.7 n	0 100	0.100	0.376
	3 7 f	0.153	0.152	0.570
	11 n	0 442	0.430	0.370
	11 f	0.664	0.645	0.553
	12 n	0.319	0.337	0.167
	12 f	0.478	0.503	0.250

For the meaning of c and **k**, see main body of text. Here "3.7 n" indicates the term in **k** corresponding to the 3.7 μm channel nadir view, "3.7 f" to 3 7 μm channel forward view, etc.

deficits in the 3.7 and 11 μm channels are comparable, while that in the 12 μm channel is smaller by a factor of about 2. The fact that the temperature deficit is always greater in the 11 μm channel than in the 12 μm channel differentiates the effect of stratospheric aerosol from that of water vapor, which depresses brightness temperatures more in the 12 μm channel than in the 11 μm channel. This is why volcanic aerosol has a large impact on traditional "split-window" retrievals [*Brown et al.*, 1997].

The effect of stratospheric aerosol on brightness temperature can be expressed algebraically as follows. Let the brightness temperatures observed or calculated in the absence of stratospheric aerosol be listed in a vector **y**. This vector may contain any desired combination of channels and look angles. Adding stratospheric aerosol changes the brightness temperatures from **y** to $\mathbf{y} + c\delta\mathbf{k}$. Here the vector **k** represents the mode of variation for the aerosol type in question, δ is the aerosol optical depth (capturing the principal dependence of the temperature deficits), and c is nearly constant (it depends weakly on the upwelling radiance). Table 1 gives the values of **k** and c (the latter being a global average value), i.e., the algebraic expression of Figure 3.

3.2. Effect of Stratospheric Aerosol on Retrieved SST

Retrieval of SST from a number of window-channel brightness temperatures is sufficiently linear to permit accurate retrieval using the equation

$$SST_{retrieved} = a_0 + \sum_{channels} a_i T_i \qquad (1)$$

where T_i is the i^{th} brightness temperature of whatever combination of channels is being considered and a_0 and the a_i are constant coefficients. This linear form has been justified by making approximations in radiative transfer [e.g., *McMillin*, 1975; *Deschamps and Phulpin*, 1980]. For convenience, we choose to use vector-matrix notation as follows: all vectors will be column vectors, and appear as lower case bold type; all matrices appear as upper case bold; and the transpose operator is superscript T. Designating the estimate of SST as $\hat{x}$, (1) can be recast as

$$\hat{x} = a_0 + \mathbf{a}^T\mathbf{y} \qquad (2)$$

The change in SST estimate associated with stratospheric aerosol can be seen by substituting $\mathbf{y} + c\delta\mathbf{k}$ for **y** in (2), and equals $c\delta\mathbf{a}^T\mathbf{k}$. The requirement for an SST retrieval to be unaffected by stratospheric aerosol is therefore that

$$\mathbf{a}^T\mathbf{k} = 0 \qquad (3)$$

Equation (3) gives us the criterion for SST retrieval to be unaffected by stratospheric aerosol, the property of "aerosol robustness." Furthermore, evaluating $c\delta\mathbf{a}^T\mathbf{k}$ gives us a means of assessing the robustness of existing retrieval coefficients. Table 2 lists values of $c\delta\mathbf{a}^T\mathbf{k}$ for previously published coefficients taken from *Závody et al.* [1995] (hereafter referred to as Z95) and *Brown et al.* [1997] (hereafter B97). (For ease of comparison, an optical depth of 0.01 has been assumed for all modes in Table 2. While this is too high for periods many years after a major eruption when aerosol is at background levels, it is not known at what age, and thus at what optical depth, the "background" mode gives a better description of aerosol effects than the "aged" mode.) In the case of the Z95 coefficients, stratospheric aerosol of optical depth 0.01 produces bias in SST of up to ~1 K. Generally, dual-look three-channel (dual-3) retrievals are much less bias prone than dual-look two-channel (dual-2) retrievals. The B97 coefficients have sensitivities ranging from the negligible (~0.01 K) to the small (~0.1 K). This degree of aerosol robustness was achieved by including varying amounts of aged volcanic aerosol in the calculations of brightness temperatures from which the coefficients were

Table 2. Robustness of selected published ATSR average SST algorithms

Algorithm		Temperature Deficit (for Optical Depth , 0.01) / K		
		Fresh volcanic	Aged volcanic	Background
Z95				
Global	dual-3	-0.19	-0.15	-0 45
	dual-2	-0.45	-0.38	-0.77
High	dual-3	-0.01	-0.01	-0.04
	dual-2	-0.22	-0 19	-0.40
Mid	dual-3	-0.19	-0.15	-0.40
	dual-2	-0.48	-0.40	-0.79
Tropical	dual-3	-0.15	-0 11	-0.29
	dual-2	-0.99	-0.82	-1 73
	nadir-3	-0.23	-0.18	-1.49
	nadir-2	-1.38	-1.08	-2 92
B97				
High	dual-3	-0 01	-0.01	-0.02
	dual-2	-0.01	-0.01	0.00
Mid	dual-3	-0.04	-0.03	-0.02
	dual-2	0.03	0.01	0.17
Tropical	dual-3	-0.04	-0.02	-0 07
	dual-2	0.01	-0.02	0.13

Results are given for center swath algorithms. "Dual-3" indicates a dual-look three-channel algorithm, etc. "High" indicates an algorithm designed for use in high latitudes, etc.

derived. This method successfully generated coefficients which are nearly robust to fresh and aged volcanic aerosol, and which are adequate for use in SST monitoring for climate studies. (B97 made no attempt to cater for background aerosol) It is, however, possible to obtain complete robustness (in a mathematical sense) by a method which is more rigorous, is simpler to implement, and which gives more insight into the nature of the problem, as we show in the next subsection.

3.3. Theory of Aerosol Robust SST Algorithms

Coefficients for a retrieval scheme based on physically modeled brightness temperatures are found by minimizing the mean square difference between the "true" SST and the "retrieved" SST given by (2), for a population of atmospheric and surface states and associated brightness temperatures calculated by radiative transfer modeling. The least squares formula given in Z95 for finding coefficients is conveniently expressed in matrix form as

$$\mathbf{a} = (\mathbf{S}_{yy} + \mathbf{S}_{\varepsilon})^{-1}\mathbf{s}_{xy}$$

$$a_0 = \bar{x} - \mathbf{a}^{\mathrm{T}}\bar{\mathbf{y}} \tag{4}$$

where a bar above a quantity indicates the mean value, x is the true SST associated with a given profile, and $\mathbf{S}_{\varepsilon}$ is the covariance matrix describing the brightness temperature noise (here taken to be diagonal, that is, noise is assumed independent between channels; forward model noise is neglected). The covariance matrix of observations $\mathbf{S}_{yy}$ and the covariance vector of SST and observations $\mathbf{s}_{xy}$ are

$$\mathbf{S}_{yy} = \overline{\mathbf{y}\mathbf{y}^{\mathrm{T}}} - \bar{\mathbf{y}}\bar{\mathbf{y}}^{\mathrm{T}}$$

$$\mathbf{s}_{xy} = \overline{x\mathbf{y}^{\mathrm{T}}} - \bar{x}\bar{\mathbf{y}}^{\mathrm{T}} \tag{5}$$

B97 used the same formulation but calculated brightness temperatures for a range of stratospheric aerosol optical thickness. This adds variability to $\mathbf{S}_{yy}$ in a manner similar to noise which is highly correlated between channels. To find fully robust coefficients, (4) must be adapted so that the linear constraint $\mathbf{a}^{\mathrm{T}}\mathbf{k}=0$ is satisfied for every stratospheric aerosol mode required. Putting the required modes $\mathbf{k}$ into a matrix of column vectors $\mathbf{K}$, it is shown in the appendix that the expression for aerosol robust coefficients is:

$$\mathbf{a} = \mathbf{S}'^{-1}_{yy}[\mathbf{s}_{xy} - \mathbf{K}(\mathbf{K}^{\mathrm{T}}\mathbf{S}'^{-1}_{yy}\mathbf{K})^{-1}(\mathbf{K}^{\mathrm{T}}\mathbf{S}'^{-1}_{yy}\mathbf{s}_{xy})] \tag{6}$$

where $\mathbf{S}'_{yy} = \mathbf{S}_{yy} + \mathbf{S}_{\varepsilon}$. Alternatively, the problem can be formulated implicitly using Lagrange multipliers [e.g., *Menke*, 1989]. The benefit of full orthogonality to the required aerosol modes comes at a cost: the SST retrieval error variance (that is, the expectation of $\{\hat{x}-x\} - \overline{\{\hat{x}-x\}}]^2$) under aerosol-free conditions is increased by

$$\Delta s_{\hat{x}} = (\mathbf{K}^{\mathrm{T}}\mathbf{S}'^{-1}_{yy}\mathbf{s}_{xy})^{\mathrm{T}}(\mathbf{K}^{\mathrm{T}}\mathbf{S}'^{-1}_{yy}\mathbf{K})^{-1}(\mathbf{K}^{\mathrm{T}}\mathbf{S}'^{-1}_{yy}\mathbf{s}_{xy}) \tag{7}$$

The usefulness of aerosol-robust coefficients depends on $\Delta s_{\hat{x}}$ being acceptably small. In general, $\Delta s_{\hat{x}}$ increases (1) as the the number of aerosol modes in $\mathbf{K}$ increases, and (2) the more similar the aerosol modes are to $\partial\mathbf{y}/\partial x$, that is, to the mode of variation associated with changes in true SST. These effects can be seen in the evaluations of (7) in Table 3. Two degrees of freedom are needed to retrieve SST in the absence of significant aerosol with a reasonable degree of atmospheric correction; this is the basis of the split window algorithm. Therefore dual 2 retrieval (using four brightness temperatures) with coefficients robust to all three aerosol types suffers an unacceptable increase in retrieval error variance. Such an algorithm can, however, be robust to one or two aerosol modes with only a modest increase in retrieval variance. Similarly, a single-view three-channel retrieval (in the nadir look direction) can be robust only to one type of aerosol without an unacceptable increase in variance. A single-3 algorithm robust to aged volcanic aerosol carries less of a penalty than one robust to background aerosol because the mode of the latter type is more similar to $\partial\mathbf{y}/\partial x$: either an increase in background aerosol loading or a decrease in SST reduces the brightness temperature most in the 3.7 μm nadir, and least in 12 μm nadir. Only dual-3 SST retrievals can be made robust to all three aerosol types without an excessive increase in retrieval error variance.

Guided by these considerations, we hereafter concentrate on developing dual-view retrieval schemes, for two and three spectral channels, which are robust to aged volcanic and background aerosol. The fresh volcanic aerosol mode can be neglected, first because it describes the aerosol present before ATSR commenced routine operation and, second, because the modes of variation associated with aged and fresh aerosol are similar; this was also noted in B97. (In fact, the bias introduced by 0.01 optical depth of fresh volcanic aerosol into SSTs derived from coefficients robust to aged and background aerosol turns out to be <0.01 K.) Lastly, we note that a scheme which is simultaneously robust to two aerosol modes is also robust to any linear combination of those modes. The ratio of aerosol temperature deficit between forward and nadir views is approximately equal for all channels and modes (Figure 3). It follows that the dual-2 scheme should be nearly robust for any stratospheric aerosol, since all will have an effect that can be approximately expressed as a linear combination of the aged and background modes. This is important given that volcanic aerosol is persistent for a few years, evolving from the aged to the background aerosol mode over this timescale. Choosing a scheme to be robust to two aerosol modes makes it less sensitive to errors in the specification of those modes.

Table 3. Increase in Retrieval Error Variance in Conditions of Negligible Stratospheric Aerosol Loading / K^2

	Type of Algorithm		
Robust Against Aerosol Type(s):	Dual-3	Dual-2	Single-3
Fresh, aged and background	0.05^2	3.5^2	—
Aged and background	$0\,04^2$	0.09^2	1.5^2
Background only	0.03^2	0.08^2	0.47^2
Aged only	0.02^2	0.08^2	$0\,12^2$

Example: if the root mean square error is 0.1 K for nonrobust coefficients and the tabulated increase in retrieval error variance is $0\,04^2$ K^2, then the resultant error for robust coefficients will be $(0.1^2 + 0.04^2)^{1/2} \sim 0.11$ K.

4. Water Vapor Continuum

Water vapor continuum absorption is the dominant absorption in the 10 to 13 μm window, and is also significant in the region of the 3.7 μm channel [*Saunders and Edwards*, 1989]. The RTM of Z95 represented the water vapor continuum absorption using the semi-empirical formulation due to *Clough et al.* [1989], referred to as "CKD_0." In this formulation, the continuum is considered to be an effect of the far wings of spectral lines broadened by both water-water and water-air collisions, giving rise to a "self" and a "foreign" component, respectively. The former is the more important in the atmospheric window regions. Standard values of self-continuum absorption cross section tabulated in wavelength are provided at two reference temperatures (260 K and 296 K), for interpolation / extrapolation to other temperatures. Updates to the

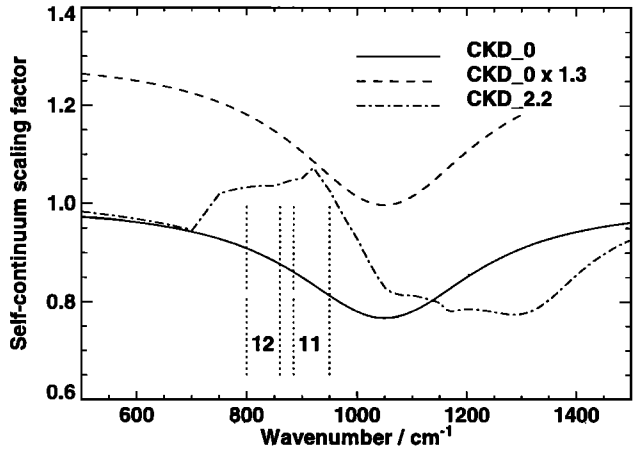

Figure 4. Relative absorption by water vapor self-continuum against wavenumber in the 11/12 μm window under three assumptions. Solid line represents scaling in the CKD_0 formulation. Broken line represents the assumption of Z95, CKD_0 scaling increased by a factor of 1.3. Dash-dotted line shows scaling in CKD_2.2. The full-width at half-maximum extent of the 11 and 12 μm channels for ATSR is indicated schematically.

continuum parameterization have consisted of various wavelength-dependent scaling factors to apply to these tabulated values.

Early in the ATSR mission, the results of aircraft measurements of water vapor continuum absorption in the tropics [*Kilsby et al.*, 1992] and of ATSR validation work [*Smith et al.*, 1994] indicated the need for revision of CKD_0 scaling factors for the 11 and 12 μm channels. A further factor of 1.3 was used by Z95 in accordance with these results. More recently, *Han et al.* [1997] have reported an updated formulation, CKD_2.2, with new scaling factors. These were derived from measurements of the downwelling thermal radiance measured by a Fourier transform spectroradiometer. These various scaling factors are presented in Figure 4. There is reasonable agreement between the CKD_2.2 continuum and the assumption of Z95 for the 11 μm channel, but the absorption in the 12 μm channel assuming CKD_2.2 is about 15% less than in Z95.

This difference in 12 μm channel absorption between the two formulations allows us to test which is more consistent with observations. There is more absorption by water vapor (lower brightness temperatures) in the 12 μm channel than in the 11 μm channel. The difference in brightness temperature between the 11 and 12 μm nadir channels will be smaller in the case of relatively less absorption in the 12 μm nadir channel, that is, in the case of CKD_2.2 being a truer formulation than CKD_0 × 1.3. We take 80 orbits of 10 arc min brightness temperature product from ATSR-2 observations (from June and July 1997, when the stratospheric aerosol loading had returned to background levels). The orbits include tracks over the warm pool region around Indonesia, where total column water vapor and upper tropospheric humidity are greatest [*Chen et al.*, 1996] and should therefore contribute maximal brightness temperature differences. We compare the distribution of 11 and 12 μm nadir differences in the real data with those predicted by radiative transfer modeling using the CKD_0 × 1.3 and CKD_2.2 formulations in Figure 5. (The spectral response functions and CO_2 concentrations appropriate to the ATSR-2 mission were used for the calculations.) Brightness temperatures are calculated for the 1358 states described in section 2 at the view angles corresponding to the center and the edge of the swath and for other across-track distances by interpolation between the center and edge brightness temperatures. This generates the simulated distributions of paired differences. The contour lines delineate contours of frequency of occurrence of brightness temperature differences. Neither distribution matches the observations precisely, partly because of different spatial and temporal sampling.

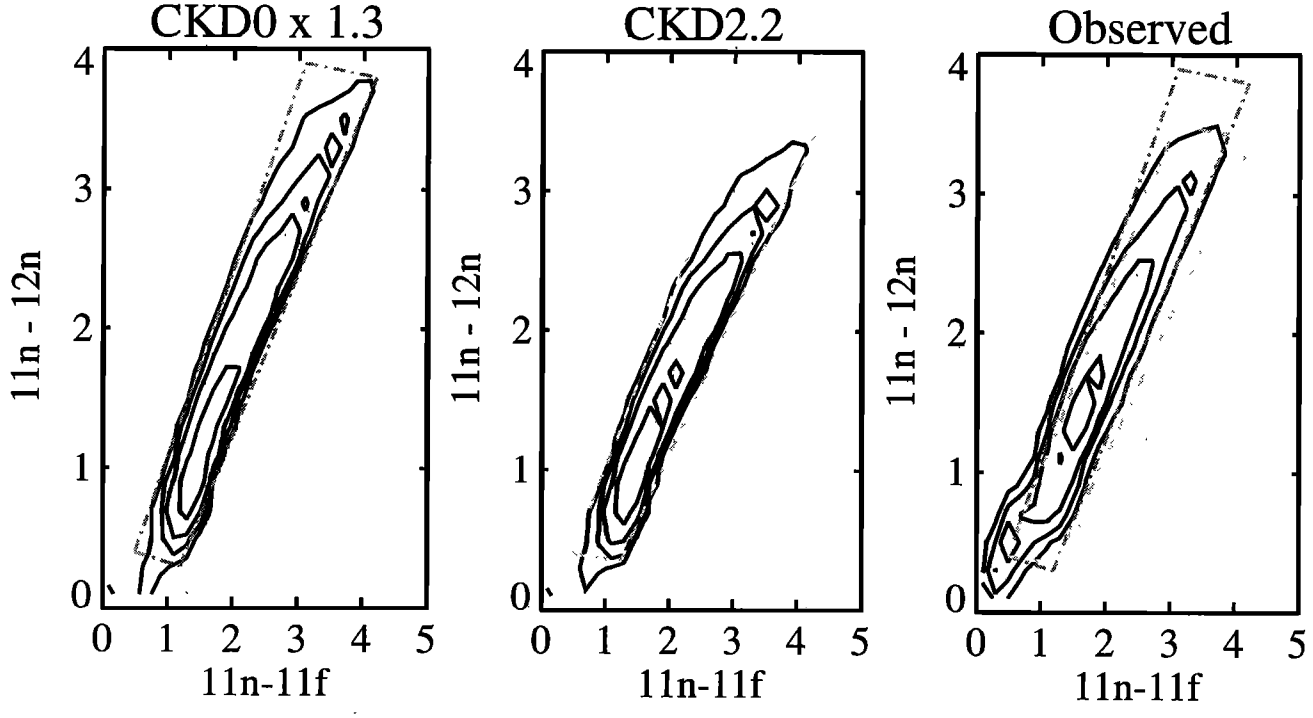

Figure 5. Modeled and observed distribution of brightness temperature differences: "11n" indictates the 11 μm channel in nadir view, "11f" the 11 μm channel in forward view; and "12n" the 12 μm channel in nadir view. The model calculations use the water vapor continuum parameterization indicated. Polygons plotted as dashed lines are to guide the eye only. Contours are drawn at frequency densities of 7%, 14%, 28%, and 70% K^{-2}.

Table 4. $\Delta \mathbf{y}$ and Corresponding Bias, From Change in Continuum Parameterization

TPW / kg m^{-2}	11 μm		12 μm		Bias / K			
	Nadir	Forward	Nadir	Forward	Z95 Dual-3	Z95 Dual-2	B97 Dual-3	B97 Dual-2
30	-0 07	-0.09	-0.22	-0.27	-0.05	-0.33	-0.03	-0.12
50	-0.15	-0.19	-0.48	-0 57	-0.11	-0.79	-0.05	-0.33

TPW, total precipitable water

Nonetheless, there are few observed 11 μm nadir -12 μm nadir differences greater than about 3.6 K. This feature is more consistent with CKD_2.2, suggesting that it may give better results at high water vapor loadings than CKD_0 × 1.3. Further evidence that CKD_2.2 represents an improvement is provided by the validation results in our companion paper [*Merchant and Harris*, this issue].

Assuming CKD_2.2 correctly models the water vapor continuum absorption, we can assess the bias caused by use of CKD_0 × 1.3 in the derivation of the Z95 and B97 retrieval coefficients. The approach is similar to that adopted to assess aerosol robustness for Table 2. We calculate $\mathbf{a}^T \Delta \mathbf{y}$, where $\Delta \mathbf{y}$ is the difference in modeled brightness temperature from use of CKD_2.2 instead of CKD_0 × 1.3. Since water vapor bias will be most important in tropical regions, we calculate a mean value of $\Delta \mathbf{y}$ for profiles with TPW in the ranges 30 ± 1 and 50 ± 1 kg m^{-2}, with the results listed in Table 4 for center of the ATSR swath. Table 4 also gives the value of $\mathbf{a}^T \Delta \mathbf{y}$ for the tropical average SST retrieval coefficients of Z95 and B97. Dual-3 retrievals are fairly robust against errors in modeling the continuum absorption in the 11 and 12 μm channels, with the modeled biases from use of CKD_0 × 1.3 being of the order of -0.1 K or less. Dual-2 retrievals are wholly dependent on the 11 and 12 μm channels and tend to have numerically larger coefficients, so the modeled biases are larger, ranging from -0.1 to -0.8 K.

5. Retrieval coefficients

We derive global coefficients designed to be robust to aged and background stratospheric aerosol by applying (6) to brightness temperatures calculated for the 1358 states using both the CKD_0 × 1.3 and CKD_2.2 formulations of water vapor continuum absorption. The coefficients are listed in Table 5.

Although the new coefficients are similar in form to those of Z95 and B97, there are differences which can be related to the introduction of robustness to stratospheric aerosol and use of CKD_2.2 in their derivation. (The changes made since Z95 and B97 in surface emissivity parameterization, atmospheric composition, treatment of aerosol scattering and distribution of profiles influence the coefficients to a lesser degree.) Since the new coefficients are global, our comparison is with the global coefficients in Table 8 of Z95. The new dual-2 coefficients place greater weight on the difference between nadir and forward brightness temperatures, obtaining robustness to stratospheric aerosol by greater reliance on geometric rather than spectral differences in optical path length (see also Figure 3). There are broadly similar differences between the regional coefficients of Z95 and those of B97 (the latter being nearly robust to aged stratospheric aerosol). B97 did not give global coefficients, so direct comparison is precluded. Comparing the new CKD_2.2 dual-2 coefficients with Z95, the sum of absolute values reduces from 19.0 to 17.4, implying slightly less noise amplification. The new CKD_2.2 dual-2 coefficients are larger than those derived using CKD_0 × 1.3 because the newer continuum parameterization tends to make the atmospheric absorption for the 12 μm channel more similar to that in the 11 μm channel. Our dual-3 coefficients also differ from those of Z95, although the weights applied to the 3.7 μm nadir and forward channels are almost identical. It is difficult to interpret the relative weightings of the other channels.

6 Retrievals of sea surface temperature

Consistency between dual-3 and dual-2 SST retrievals is a requirement of an ideal retrieval scheme. In this section therefore we use this requirement to appraise various ATSR SST retrieval schemes, including the new coefficients developed by incorporating the improvements we have described in previous sections. Validation of the absolute retrieval accuracy of our new algorithms is treated in our companion paper [*Merchant and Harris*, this issue].

Table 5. New Dual-View Retrieval Coefficients

	a_0	3.7 n	3 7 f	11 n	11 f	12 n	12 f
CKD_0 × 1.3							
Dual-2 center	5.72			6.16363	-3.64183	-3.85214	2.30807
Dual-2 edge	6.33			7 54247	-5.05434	-4.68443	3 17197
Dual-3 center	0.71	2 51631	-1.47839	0.63417	-0.33124	-0.73272	0.38884
Dual-3 edge	0.75	3.18424	-2.12442	0.60933	-0.36008	-0.79370	0 48124
CKD_2.2							
Dual-2 center	6.81			6.59144	-3.89459	-4.29377	2.57103
Dual-2 edge	7.55			8.05214	-5.39440	-5.20973	3.52359
Dual-3 center	0.40	2.72688	-1.60794	0.26418	-0.09649	-0.54805	0.25954
Dual-3 edge	0.99	3 20655	-2.14282	0.71074	-0.42027	-0.90759	0.54913

Here "3.7 n" denotes the coefficient multiplying the 3.7 μm nadir brightness temperature, "3.7 f," the 3.7 μm forward brightness temperature coefficient, etc.

The ATSR Data Processing Group at the Rutherford Appleton Laboratory (UK) provided brightness temperature data for two months from the first year of the ATSR mission, covering September to October 18, 1991 and April 22 to May 26, 1992. These represent the first cycle of routine ATSR operation, and the last 35 days before the failure of the 3.7 μm channel. ERS-1 followed a 3-day repeat pattern during the former period (giving incomplete coverage) and a 35-day repeat cycle during the latter period (giving complete coverage). The data are averaged cloud-cleared brightness temperatures located on a $^1/_6^\circ$ latitude-longitude grid. Since 3.7 μm channel brightness temperatures are not available from ATSR during the daytime, only nighttime data are used in this comparison. For each month, the utilized data amount to about 1.5 million sets of six spatially averaged brightness temperatures (ABTs) with associated temporal, spatial, and confidence data. The spatial data include the mean across-track distance of the nadir cloud-cleared brightness temperatures contributing to the ABT. This mean across-track distance is used in interpolating between the center and edge retrieval coefficients, as described by *Harris and Saunders* [1996].

We apply various dual-3 and dual-2 SST retrieval schemes to these observed data. First is the prelaunch scheme (Z95), based on coefficients derived for three latitude regions and five across-track bands. Second is the aerosol robust average SST scheme of B97. Third is the new global scheme introduced in section 5, based on the improved RTM and set of states (section 2), applying the new technique for incorporating aerosol robustness (section 3) and using interpolation across track, but in one case retaining the continuum assumed in both Z95 and B97 (CKD_0 × 1.3), and in the other case using CKD_2.2 (see section 4).

The consistency of the retrieval schemes will be assessed using the bias (the mean value of the dual-2 minus dual-3 SST) and standard deviation (the root of the variance of the same difference). The global bias should be zero. The standard deviation of the retrievals should approach the best possible given the distribution stratospheric aerosol loadings. *Murray et al.* [1998a] have approximately quantified the minimum possible standard deviations by obtaining dual-2 coefficients (and the corresponding SSTs) by regression to Z95 dual-3 SST retrievals for the same ABT data (using three latitude zones). The resulting minimum standard deviations were 0.22 K and 0.24 K for the September-October 1991 and April-May 1992 data, respectively.

In Table 6, the bias and standard deviation of dual-2 minus dual-3 SST retrievals for the ABT data are shown for various retrieval schemes. All aerosol-robust schemes have considerably less bias and markedly smaller standard deviation than the prelaunch retrieval scheme. B97 does particularly well for the September-October 1991 ABT data, with almost no bias and near-optimum standard deviation. For April-May 1992, it is less successful, developing a bias of more than 0.1 K and a standard deviation significantly greater than the optimum. Both new schemes give a standard deviation closely approaching the optimum for both time periods, despite being aerosol robust for two aerosol types and having a single set of coefficients applied globally. The CKD_2.2 scheme gives smaller biases than the CKD_0 × 1.3 scheme, although both schemes show the same change in bias between the two time periods of -0.08 K. We conclude that both our incorporation of aerosol robustness and use of the updated description of water vapor continuum absorption yield better retrievals. Adopting the SSTs retrieved using new dual-3 scheme with CKD_2.2 as "reference" SSTs (that is, our best estimates of the true SSTs), we can deduce that the global mean bias in dual-2 SSTs using the prelaunch scheme relative to the true skin SST is about -0.8 K, of which -0.1 to -0.2 K arises from use of the CKD_0 × 1.3 continuum parameterization. This depends, of course, on the truth of the reference SST. A high degree of confidence in the reference SST is justified partly because of the excellent consistency arising from our improvements to the RTM and states used, and partly because dual-3 retrievals are, by their nature, fairly stable against mis-specification of the state or behaviour of the atmosphere [*Mutlow et al.*, 1994; *Murray et al.*, 1998b]. The mean and standard deviation of the difference between dual-3 SSTs from the prelaunch and "New, CKD_2.2" schemes are 0.09 K and 0.10 K respectively, with the prelaunch values cooler.

The global distribution of improvements in the consistency of dual-2 SSTs with the reference SST retrievals is illustrated in Plate 1. In Plate 1a, the effect of Pinatubo aerosol on the SST retrievals is clearly visible as the band of relative bias of up to -2.0 K in the equatorial region. The aerosol loading at the equator reduced by ~50% by April-May 1992, partly by poleward dispersal of the aerosol; this accounts for the smaller equatorial and greater midlatitude bias in Plate 1d. Although there is a negative shift in bias of about 0.08 K at all longitudes and latitudes between Plates 1b and 1e, these plots for the aerosol-robust scheme with the CKD_0 × 1.3 continuum parameterization have a similar pattern and relative magnitude of bias in equatorial regions. This suggests an origin other than stratospheric aerosol for this pattern of bias (and hence

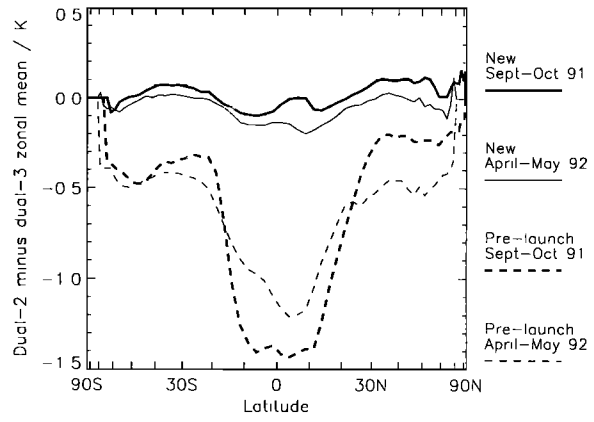

Figure 6. Zonal mean bias with respect to reference SSTs of dual-2 retrievals (new, using CKD_2.2, and prelaunch). The horizontal scale is such that the spacing between any two latitudes is proportional to the area of Earth's surface between them.

Table 6: Bias and Standard Deviation of Dual-2 Minus Dual-3 SSTs

Dual-View Two-Channel SST Scheme	Dual-View Three-Channel SST Scheme	Sep.-Oct 1991		April-May 1992	
		Bias	s.d.	Bias	s.d.
Prelaunch (Z95)	Prelaunch (Z95)	-0.67	0 57	-0.70	0.48
B97	B97	-0.01	0.23	-0.12	0.29
New, CKD_0 × 1.3	New, CKD_0 × 1.3	-0.10	0.22	-0.18	0.25
New, CKD_2.2	New, CKD_2 2	0.02	0.22	-0 06	0.25
Prelaunch (Z95)	New, CKD_2.2	-0.77	0.67	-0.79	0.51
B97	New, CKD_2.2	-0.07	0.25	-0 18	0.30
New, CKD_0 × 1.3	New, CKD_2.2	-0.15	0 24	-0.24	0.28

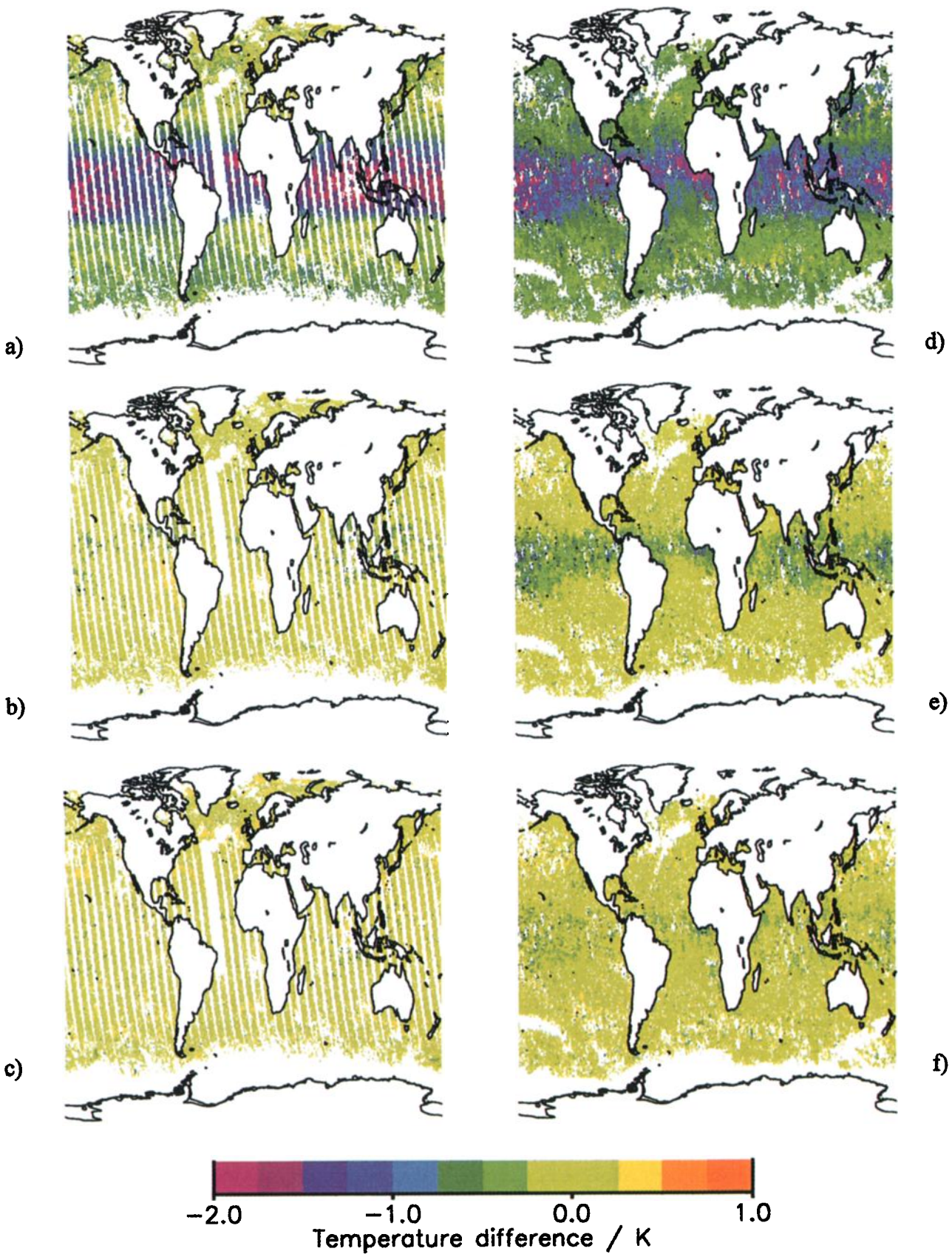

Plate 1. Estimated bias in dual-view two-channel SST retrievals (mean difference from reference SST retrievals). (a to c) September-October 1991 ABT data: (a) prelaunch scheme, (b) aerosol-robust scheme, CKD_0 continuum, (c) aerosol-robust scheme, CKD_2.2 continuum. (d to f) , April-May 1992 ABT data: (d) prelaunch scheme, (e) aerosol-robust scheme, CKD_0 continuum, (f) aerosol-robust scheme, CKD_2.2 continuum.

that the scheme is aerosol robust), with an inadequate atmospheric water vapor correction being the most obvious candidate cause, since these equatorial regions have high water vapor loadings. Residual traces of this pattern remain in the corresponding Plates 1c and 1f, but with the relative size of the bias reduced. These latter figures are for an aerosol-robust scheme using the CKD_2.2 continuum, so this confirms the suggested role of water vapor in the residual biases seen in Plates 1b and 1e. The pattern of small residual bias in Plates 1c and Plates 1f indicates that the CKD_2.2 continuum parameterization, although a marked improvement, is likely to require further modification.

The dual-2 retrievals are more negative compared to reference SSTs when applied to the April-May ABTs than the September-October ABTs. As can be seen in Figure 6, the shift in relative bias occurs at all latitudes between 60°S and 60°N. At latitudes poleward of 60°N or S, the interseasonal variability makes comparison between spring and autumn more difficult. The presence of the shift at all latitudes suggests a cause other than changing aerosol loadings or water vapor amounts. Current understanding of instrumental drifts over this period cannot explain a shift of more than 0.02 K. Neither the ~5 ppmv (peak-to-peak) annual variation nor the ~1.5 ppmv yr^{-1} increase in global CO_2 concentration could account for a shift of more than 0.001 K. The origin of this shift in relative bias therefore remains a matter for investigation. Figure 6 also clarifies the latitudinal structure of the improvement brought by use of the new coefficients compared to the prelaunch coefficients.

7. Discussion

Our objective has been the elimination of bias in retrievals of SST from ATSR. The techniques we have developed and applied represent considerable progress toward that objective. The prelaunch retrieval scheme was affected by major biases in dual-view two-channel retrievals, from the presence of volcanic aerosol in the stratosphere, and from inadequate modeling of the water vapor continuum absorption in the 11 and 12 μm channels. Our method of ensuring that retrieval coefficients are aerosol robust and our more accurate and representative set of modeled brightness temperatures have greatly improved the consistency of dual-view two-channel and dual-view three-channel retrievals. This consistency is of particular importance, since the 3.7 μm channel failed in May 1992, so only two-channel retrievals are possible thereafter. Global mean differences are reduced from ~0.7 K to ~0.04 K, and the global standard deviation of differences reduced from ~0.5 K to ~0.25 K. Moreover, these results have been obtained using a single set of global coefficients rather than using different coefficients for different latitude zones. For dual-view SST retrievals, we find that latitude-dependent coefficients give little improvement in random error.

Despite the considerable progress presented in this paper, some issues remain to be resolved. A shift in the relative bias of dual-view two-channel to dual-view three-channel SSTs of -0.08 K occurred between September-October 1991 and April-May 1992. The origin of this shift in relative bias is under investigation. In most oceanographic contexts, it is a very small concern. In the context of using ATSR data in climate change detection, which requires stability of ~0.1 K per decade, it is clearly significant. This illustrates the extremely demanding requirements for use of satellite data in climate change monitoring. Despite the unrivaled calibration and noise characteristics of ATSR and the detailed physical modeling presented in this paper, in the context of climate change detection, the residual trend in dual-view two-channel SST retrievals is unacceptable. Research into the elimination of artefactual trends in the ATSR SST record continues, and part of the remit of that research must be to examine how best to bring information from in situ measurements into the retrieval process to eliminate spurious trends, while retaining the advantages that a scheme based on physical modeling has over purely empirical methods.

Meanwhile, results of an exercise to compare retrievals with in situ measurements [*Merchant and Harris*, this issue] support the view that the new retrieval coefficients are indeed robust to the effects of the Pinatubo aerosol and deal with high water vapor loadings better than previous retrieval coefficients. The comparison exercise also raises avenues for further work. First, it suggests that further work on minimizing the effects of residual cloud contamination of brightness temperatures is required if dual-2 retrievals are to attain an accuracy of better than 0.3 K. Second, it suggests that a warm bias of 0.2 K is present in dual-3 retrievals, after taking account of skin-bulk temperature differences. Although this is a small bias, and could easily be corrected empirically (by adjusting the offset coefficient, a_0), it would be preferable to understand its origin and correct it by improved physical modeling.

For clarity, we have restricted the results presented in this paper to dual-view retrievals, which are available only from the ATSR. Some comments are appropriate on the relevance of our work to single-view retrievals and AVHRR. First, we note that our calculations using (7) listed in Table 3 show that single-view three-channel SST retrievals can be rendered robust to aged volcanic aerosol with a modest increase in SST retrieval variance of the order of $0.1^2\,K^2$. The question of the biases in AVHRR (single-view) SSTs from the Pinatubo aerosol was addressed by *Reynolds* [1993]. Reynolds describes how changing the operational retrieval scheme after the manner of *Walton* [1985] reduced differences between satellite and in situ SSTs in September-October 1991 from -1.3 to -0.5 K. In principle, the method we have given could render such residual bias even smaller. Since single-view three-channel retrieval coefficients can be orthogonal to only one aerosol mode, however, this depends critically on that mode representing accurately the effect of the stratospheric aerosol. We developed a global single-view retrieval scheme which was nominally robust to aged volcanic aerosol for ATSR. When applied to the September-October ABTs, the global bias with respect to the reference SST retrievals was -0.4 K. While this improves to -0.3 K if latitude-dependent coefficients are used, attaining high degrees of aerosol-robustness is clearly more difficult for single-view observations. This is because more accurate knowledge of the aerosol spectral properties is required. As noted by *Walton* [1985] and B97, single-view observations at 11 and 12 μm only cannot be made aerosol robust. The success of dual-view retrieval schemes is due to the forward-view components of the aerosol mode vector being related to the corresponding nadir-view components by optical path increases determined by geometry rather than the spectral properties of the absorber.

Lastly, we note that the reprocessing to SST of data from the ERS-1 ATSR mission by the Rutherford Appleton Laboratory is ongoing during 1999. New dual-view retrieval coefficients derived as described in this paper are being used for this reprocessing program, for both averaged and pixel-resolution SST products.

Appendix

The constraint $\mathbf{a}^T\mathbf{k} = 0$ must hold for each mode $\mathbf{k}$ for which robustness is required. Putting the required modes into a matrix of column vectors $\mathbf{K}$ this becomes

$$\mathbf{K}^T\mathbf{a} = \mathbf{0} \tag{A1}$$

where the ordering is chosen such that the zero vector **0** is a column vector according to the chosen convention. Equation (A1) expresses the constraint(s) required to be placed on the retrieval coefficients. Coefficients satisfying these constraints can be found using the textbook method of Lagrange multipiers [e.g., *Menke*, 1989]. Briefly, to minimize the retrieval error $\sigma_{\hat{x}}^2$ with respect to the coefficients **a** subject to the constraint(s) (A1), the method is to solve simultaneously

$$\frac{\partial}{\partial \mathbf{a}}\left(\frac{1}{2}\sigma_{\hat{x}}^2 + \Lambda^{\mathrm{T}}(\mathbf{K}^{\mathrm{T}}\mathbf{a})\right) = \mathbf{0}$$

$$\mathbf{K}^{\mathrm{T}}\mathbf{a} = \mathbf{0} \qquad \text{(A2)}$$

where Λ is a vector of Lagrange multipliers, one element for each constraint, and the constant premultiplying $\sigma_{\hat{x}}^2$ is arbitrary and chosen for convenience. It can be shown by evaluating $\sigma_{\hat{x}}^2 = \langle(\hat{x} - x - \langle\hat{x} - x\rangle)^2\rangle$ for arbitrary coefficients **a** that

$$\sigma_{\hat{x}}^2 = \overline{x^2} - \bar{x}^2 + \mathbf{a}^{\mathrm{T}}\mathbf{S}'_{yy}\mathbf{a} - 2\mathbf{a}^{\mathrm{T}}\mathbf{s}_{xy} \qquad \text{(A3)}$$

and since

$$\frac{\partial}{\partial \mathbf{a}}(\overline{x^2} - \bar{x}^2 + \mathbf{a}^{\mathrm{T}}\mathbf{S}'_{yy}\mathbf{a} - 2\mathbf{a}^{\mathrm{T}}\mathbf{s}_{xy}) = 2\mathbf{S}'_{yy}\mathbf{a} - 2\mathbf{s}_{xy} \qquad \text{(A4)}$$

it follows that (A2) is equal to

$$\mathbf{S}'_{yy}\mathbf{a} - \mathbf{s}_{xy} + \mathbf{K}\Lambda = \mathbf{0}$$

$$\mathbf{K}^{\mathrm{T}}\mathbf{a} = \mathbf{0} \qquad \text{(A5)}$$

Premultiplying the first line by $\mathbf{K}^{\mathrm{T}}\mathbf{S}'^{-1}_{yy}$ and substituting the second line gives:

$$-\mathbf{K}^{\mathrm{T}}\mathbf{S}'^{-1}_{yy}\mathbf{s}_{xy} + \mathbf{K}^{\mathrm{T}}\mathbf{S}'^{-1}_{yy}\mathbf{K}\Lambda = \mathbf{0}$$

$$\Rightarrow \Lambda = (\mathbf{K}^{\mathrm{T}}\mathbf{S}'^{-1}_{yy}\mathbf{K})^{-1}\mathbf{K}^{\mathrm{T}}\mathbf{S}'^{-1}_{yy}\mathbf{s}_{xy} \qquad \text{(A6)}$$

Substituting this value of Λ into the top line of (A5) and rearranging finally yields the required result (6) for coefficients which are orthogonal to the specified aerosol modes

$$\mathbf{a} = \mathbf{S}'^{-1}_{yy}[\mathbf{s}_{xy} - \mathbf{K}(\mathbf{K}^{\mathrm{T}}\mathbf{S}'^{-1}_{yy}\mathbf{K})^{-1}(\mathbf{K}^{\mathrm{T}}\mathbf{S}'^{-1}_{yy}\mathbf{s}_{xy})] \qquad \text{(A7)}$$

Acknowledgments. Chris Merchant is funded by the U.K. Natural Environment Research Council (NERC) on doctoral studentship GT4/95/210D, a CASE award with the U.K. Meteorological Office. Andy Harris is funded under the Climate Prediction Programme of the UK Department of the Environment, Transport and the Regions. ATSR data were produced by the ATSR Data Processing Group at the Rutherford Appleton Laboratory, funded by NERC, and are courtesy of RAL / NERC / ESA / BNSC. The provision of European Centre for Medium-range Weather Forecasting Reanalysis data by the British Atmospheric Data Centre is gratefully acknowledged. We thank the anonymous referees for their help in improving this paper.

References

Allan, R., J. Lindesay, and D. E. Parker, *El Nino Southern Oscillation and Climatic Variability*, CSIRO Publishing, Melbourne, Victoria, Australia, 1996.

Allen, M. R., C. T. Mutlow, G. M. C. Blumberg, J. R. Christy, R. T. McNider, and D. T. Llewellyn-Jones, Global change detection, *Nature, 370*, 24-25, 1994.

Balagurov, A., A. Kats and N. Krestyannikova, Implementation and results of the WMO radiosondes humidity sensors intercomparison - Phase I "Laboratory Test," Proceedings of the WMO Technical Conference on Meteorological and Environmental Instruments and Methods of Observation (TECO-98), WMO instruments and observing methods, *Rep. 70*, pp. 181-184, World Meteorol. Organ., Geneva, 1998.

Baran, A. J., and J. S. Foot, New application of the operational sounder HIRS in determining a climatology of sulfuric acid aerosol from the Pinatubo eruption, *J. Geophys. Res., 99*, 25 673-25 679, 1994.

Barton, I. J., A. J. Prata, and R. P. Cechet, Validation of the ATSR in Australian waters, *J. Atmos. Oceanic Technol., 12*, 290-300, 1995.

Bluth, G. J. S., S. D. Doiron, C. C. Schnetzler, A. J. Krueger, and L. S. Walter, Global tracking of the SO_2 clouds from the June 1991 Mount Pinatubo eruptions, *Geophys. Res. Lett., 19*, 151-154, 1992.

Brown, S. J., A. R. Harris, I. M. Mason, and A. M. Zavody, New aerosol-robust sea surface temperature algorithms for the along-track scanning radiometer, *J. Geophys. Res., 102*, 27,973-27,990, 1997.

Chen, C.-T., E. Roeckner, and B. J. Soden, A comparison of satellite observations and model simulations of column-integrated moisture and upper-tropospheric humidity, *J. Clim., 9*, 1561-1585, 1996.

Clough, S. A., F. X. Kneizys, and R. W. Davies, Line shape and the water vapor continuum, *Atmos. Res., 23*, 229-241, 1989.

Delderfield, J., D. T. Llewellyn-Jones, R. Bernard, Y. de Javel, E. J. Williamson, I. M. Mason, D. R. Pick, and I. J. Barton, The along track scanning radiometer (ATSR) for ERS-1, *Proc. SPIE Int. Soc. Opt. Eng., 589*, 114-120, 1986.

Deschamps, P. Y. and T. Phulpin, Atmospheric correction of infrared measurements of sea surface temperature using channels and 3.7, 11 and 12 μm, *Boundary Layer Meteorol., 18*, 131-143, 1980.

Hamill, P., E. J. Jensen, P. B. Russell, and J. J. Baumann, The life cycle of stratospheric aerosol particles, *Bull. Am. Meteorol. Soc., 90*, 1395-1410, 1997.

Han, Y., J. A. Shaw, J. H. Churnside, P. D. Brown, and S. A. Clough, Infrared spectral radiance measurements in the tropical Pacific atmosphere, *J. Geophys. Res., 102*, 4353-4356, 1997.

Harris, A. R., and M. A. Saunders, Global validation of the along-track scanning radiometer against drifting buoys, *J. Geophys. Res., 101*, 12,127-12,140, 1996.

Jones M. S., M. A. Saunders, and T. H. Guymer, Global remnant cloud contamination in the along-track scanning radiometer data: Source and removal, *J. Geophys. Res., 101*, 12,141-12,147, 1996.

Kilsby, C. G., D. P. Edwards, R. W. Saunders, and J. S. Foot, Water-vapor continuum absorption in the tropics:Aircraft measurements and model comparisons, *Q. J. R. Meteorol. Soc., 118*, 715-748, 1992.

Lambert, A., R. G. Grainger, J. J. Remedios, C. D. Rodgers, M. Corney, and F. W. Taylor, Measurements of the evolution of the Mt. Pinatubo aerosol cloud by ISAMS, *Geophys. Res. Lett., 20*, 1287-1290, 1993.

Mason, I. M., P. H. Sheather, J. A. Bowles and G. Davies, Blackbody calibration sources of high accuracy for a spaceborne infrared instrument: The Along Track Scanning Radiometer, *Appl. Opt., 35*, 629-639, 1996.

Masuda, K., T. Takashima, and Y. Takayama, Emissivity of pure and sea waters for the model sea surface temperature in the infrared regions, *Remote Sens. Environ., 24*, 313-329, 1988.

May, D. A., and R. J. Hoyler, Sensitivity of satellite multichannel sea surface temperature retrievals to the air-sea temperature difference, *J. Geophys. Res., 98*, 12,567-12,577, 1993.

McClain, E. P., Global sea surface temperatures and cloud clearing for optical depth estimates, *Int. J. Remote Sens., 10*, 763-769, 1989.

McClain, E. P., W. G. Pichel, and C. C. Walton, Comparative performance of AVHRR-based multichannel sea surface temperatures, *J. Geophys. Res., 90*, 11,578-11,601, 1985.

McCormick M. P., and R. E. Veiga, SAGE II measurements for early Pinatubo aerosols, *Geophys. Res. Lett., 19,* 155-158, 1992.

McCormick, M. P., P.-H. Wang and L. R. Poole, Stratospheric aerosols and clouds, *Aerosol-Cloud-Climate Interactions,* edited by P. V. Hobbs, *Int. Geophys. Ser.*, vol. 54, Academic, San Diego, Calif., 1993.

McMillin, L.M., Estimation of sea surface temperature from two infrared window measurements with differential absorption, *J. Geophys. Res., 80,* 5113-5117, 1975.

Menke, W., *Geophysical Data Analysis: Discrete Inverse Theory,* rev. ed., pp. 55-57, *Int. Geophys. Ser.*, vol. 45, Academic, San Diego, Calif., 1989.

Merchant, C. J., and A. R. Harris, Towards the elimination of bias in satellite retrievals of sea surface temperature, 2. Comparison with in situ measurements, *J. Geophys. Res.*, this issue.

Minnett, P.J., A numerical study of the effects of anomalous North Atlantic atmospheric conditions on the infrared measurement of sea surface temperature from space, *J. Geophys. Res., 91,* 8509-8521, 1986.

Minnett, P. J., The regional optimization of infrared measurements of sea surface temperature from space, *J. Geophys. Res., 95,* 13,497-13,510, 1990.

Murray, M. J., M. R. Allen, C. J. Merchant, and A. R. Harris, Potential for improved dual-view SST retrievals from ATSR, *Geophys. Res. Lett., 25,* 3363-3366, 1998a.

Murray, M. J., M. R. Allen, C. T. Mutlow, A. M. Závody, M. S. Jones and T. N. Forrester, Actual and potential information in dual-view radiometric observations of sea surface temperature from ATSR, *J. Geophys. Res., 103,* 8153-8165, 1998b.

Mutlow, C. T., A. M. Závody, I. J. Barton, and D. T. Llewellyn-Jones, Sea surface temperature measurements by the along-track scanning radiometer on the ERS-1 satellite: Early results, *J. Geophys. Res., 99,* 575-588, 1994.

Reynolds, R. W., Impact of Mount Pinatubo aerosol on satellite-derived sea surface temperatures, *J. Clim., 6,* 768-774, 1993.

Saunders, R. W., and D. P. Edwards, Atmospheric transmittances for the AVHRR channels, *Appl. Opt., 28,* 4154-4160, 1989.

Schmidlin, F.J., Summary of the WMO international radiosonde relative humidity sensor comparison - Sep. 1995, - Phase II "Field Test", Proceedings of the WMO Technical Conference on Meteorological and Environmental Instruments and Methods of Observation (TECO-98), WMO instruments and observing methods, *Rep. 70,* pp. 185-187, World Meteorol. Organ., Geneva, 1998.

Smith, A. H., R. W. Saunders, and A. M. Závody, The validation of ATSR using aircraft radiometer data over the tropical atlantic, *J. Atmos. Oceanic Technol., 11,* 789-800, 1994.

Soden, B.J. and F.P. Bretherton, Evaluation of water vapor distribution in general circulation model using satellite observations, *J. Geophys. Res., 99,* 1187-1210, 1994.

Soden, B.J., and J.R. Lanzante, An assessment of satellite and radiosonde climatologies of upper-tropospheric water vapor, *J. Clim., 9,* 1235-1250, 1996.

Thomas, J. P., and J. Turner, Validation of Atlantic Ocean sea surface temperatures measured by the ERS-1 Along Track Scanning Radiometer, *J. Atmos. Oceanic Technol., 12,* 1303-1312, 1995.

Trepte, C. R., R. E. Veiga, and M. P. McCormick, The poleward dispersal of Mount Pinatubo volcanic aerosol, *J. Geophys. Res., 98,* 18,563-18,573, 1993.

Walton, C., Satellite measurement of sea surface temperature in the presence of volcanic aerosols, *J. Clim. Appl. Meteorol., 24,* 501-507, 1985.

Watson R. T., L. G. Meira Filho, E. Sanhueza and A. Janetos, Greenhouse gases: Sources and sinks, in *Climate Change 1992: The Supplementary Report to the IPCC Scientific Assessment,* edited by J. T. Houghton, B. A. Collander, and S. K. Varney, Intergovt. Panel on Clim. Change, Geneva, 1992.

Watts, P. D., M. R. Allen, and T. J. Nightingale, Wind speed effects on sea surface emission and reflection for the Along Track Scanning Radiometer, *J. Atmos. Oceanic Technol., 13,* 126-141, 1996.

Webster, P. J., The role of hydrological processes in ocean-atmosphere interactions, *Rev. Geophys., 32,* 427-476, 1994.

Závody, A. M., C. T. Mutlow, and D. T. Llewellyn-Jones, A radiative transfer model for sea surface temperature retrieval for the along-track scanning radiometer, *J. Geophys. Res., 100,* 937-952, 1995.

A. R. Harris, U.K. Meteorological Office, London Road, Bracknell, Berks, RG12 2SZ, England, U.K. (arharris@meto.gov.uk)

C. J. Merchant, Department of Meteorology, The University of Edinburgh, James Clerk Maxwell Building, The King's Buildings, Mayfield Road, Edinburgh, EH9 3JZ, Scotland, U.K. (chris@met.ed.ac.uk)

M. J. Murray, Space Science Department, Rutherford Appleton Laboratory, Chilton, Didcot, OX11 0QX, England, U.K. (Jo.Murray@rl.ac.uk)

A. M. Závody, Albinus Ltd, 42 Buckland Ave., Slough, SL3 7PH, England, U.K. (albin@zavody.freeserve.co.uk)

(Received August 4, 1998; revised March 1, 1999;
accepted March 30, 1999.)